CONF-9409376--1
SAND95-2194C

High Silicon Content Silylating Reagents for Dry-Developed Positive-Tone Resists for Extreme Ultraviolet (13.5 nm) and Deep Ultraviolet (248 nm) Microlithography

David Wheeler, Eric Scharrer, Glenn Kubiak
Sandia National Labs[1], Albuquerque, NM 87185-0368.

Richard Hutton, Susan Stein, Ray Cirelli, Frank Baiocchi, May Cheng, Craig Boyce, Gary Taylor.
AT&T Bell Laboratories, Murray Hill, N.J. 07974-0636.

Abstract

Recent results in the use of disilanes as silylating reagents for near-surface imaging with deep-UV (248 nm) and EUV (13.5 nm) lithography are reported. A relatively thin imaging layer of a photo-cross-linking resist is spun over a thicker layer of hard-baked resist that functions as a planarizing layer and antireflective coating. Photoinduced acid generation and subsequent heating crosslinks and renders exposed areas impermeable to an aminodisilane that reacts with the unexposed regions. Subsequent silylation and reactive ion etching afford a positive-tone image. The use of disilanes introduces a higher concentration of silicon into the polymer than is possible with silicon reagents that incorporate only one silicon atom per reactive site. The higher silicon content in the silylated polymer increases etching selectivity between exposed and unexposed regions and thereby increases the contrast. Additional improvements that help to minimize flow during silylation are also discussed, including the addition of bifunctional disilanes. We have resolved high aspect ratio, very high quality 0.20 μm line and space patterns at 248 nm with a stepper having a numerical aperture (NA)= 0.53, and have resolved ≤ 0.15 μm line and spaces at 13.5 nm.

DISCLAIMER

Portions of this document may be illegible in electronic image products. Images are produced from the best available original document.

Introduction:

Design rules for microlithography are moving into the sub 0.35 μm regime. This generates more stringent requirements for the entire lithographic process. Deep UV (248 nm) lithography has demonstrated the ability to print sub 0.35 μm features. However, deep UV lithography at 248 nm will probably be unable to meet the design rules that are expected to be needed at the turn of the century. To meet these needs, exposure tools will probably employ shorter wavelength radiations. Extreme ultraviolet lithography, EUVL, at 13.5 nm has demonstrated the capability to print very fine features, and it is predicted that the trend to shorter wavelengths will eventually employ 13.5 nm radiation about the year 2010. Unfortunately, radiation at 13.5 nm, formerly called soft x-ray lithography, is strongly attenuated by almost all materials. Since very thin films are not adequate for the manufacture of devices, some sort of surface imaging scheme will be needed for EUVL resists. Even 193 nm lithography may require surface imaging techniques due to the high absorption of most photoresists at this wavelength. While there are a few photoresist materials for 193 nm lithography that are transparent enough to allow imaging in a single layer, there are no such materials for EUV lithography. This is due to the atomic nature of the absorption for EUV as opposed to the molecular absorption for deep UV wavelengths. Surface imaging provides a method for overcoming the problems of optical density, but introduces additional processing variables. However, surface imaging relaxes many of the other processing issues and requirements such as those associated with topography and reflection.

Surface imaging schemes can be broken down into two basic categories based on the thickness of material used for imaging. Near surface imaging schemes are typified by processes such as DESIRE[2] and SAHR[3], which utilize the top few thousand angstroms of resist. At-the-surface-imaging schemes employ only the uppermost 100Å and are typified by such processes as the recently described photo-definable electroless nickel deposition process.[4] We recently described a near surface imaging scheme that employed disilanes and a bilayer resist scheme to improve silicon contrast (Figure 1).[5]

The rational for choosing to examine disilanes can be seen in Table 1. A summary of commonly used mono- and difunctional silylating agents is shown in Table 1. The swelling was calculated from the change in number of atoms in the repeat unit of the polymer realative to the number of atoms in the silylated polymer. While admittedly simplistic, the calculations matched experimental results fairly closely. Experimentally measured volume increases were smaller than calculated.

This is probably due to the fact that photoresists are not pure polymers and contain species which are not involved in silylation. Difunctional silylating agents were assumed to react completely for the calculations. From the table it is clear that despite the higher boiling points, disilanes hold the promise of large weight percent silicon incorporation without enormous swelling. It is further evident that pure difunctional silylating agents, while causing little swelling, add little silicon to the resist. Increasing the silicon content increases the etch selectivity and processing latitudes.

Our silylation scheme is similar to the SAHR process. Briefly, it employs photoinduced acid generation in the top imaging layer and subsequent post exposure baking to crosslink the acid-containing regions and render these areas impermeable and unreactive to N,N-dimethylaminopentamethyldisilane, (DMAPMDS). This disilane, despite a boiling point of 155 °C and large steric size, is as reactive under our silylation conditions as hexamethyldisilazane. A brief chlorine/argon descum followed by reactive ion etching transfers the surface pattern into the bulk of the resist. By employing etching conditions that effect both sidewall deposition and etching at the same time, nearly vertical side walls can be achieved with minimum undercut.[6] The descum step is needed since there is some silylation, approximately 200 Å, of the crosslinked areas. The descum step removes all residue and improves the reproducibility and linearity of the process. We believe that the surface silylation in the crosslinked areas occurs because of acid loss during post exposure baking by volatilization from the surface of the resist.

Synthesis of Disilanes:

Most of our work has been with N,N-dimethylaminopentamethyldisilane (DMAPMDS). Two syntheses of this material are shown in Equation 1. A single methyl group of hexamethyldisilane, Me_6Si_2, can be replaced with a chlorine by reacting the disilane with excess sulfuric acid followed by ammonium chloride (65% yield).[7] This we termed the sulfuric acid (SA) route. Alternatively, Me_6Si_2 reacts with an equivalent of triflic acid to give pentamethyldisilyl triflate (80%). We term this the triflic acid (TA) route. A second equivalent of triflic acid gives 1,1,2,2-tetramethyldisilane ditriflate in a somewhat lower yield.[8] Aminolysis with excess dimethylamine or methylamine gives the aminodisilane (>80%). The reaction of trifilic acid with hexamethyldisilane can be carried out neat. The reaction can therefore be carried out in a single pot. While aminolysis of the ditriflate gives 1,2-bis(N,N-dimethylamino)tetramethyldisilane, we have found that it is easier to synthesize it from the dichloride. The dichloride is available in over 95% yield from the reaction of two equivalents of the aluminum

trichloride and acetyl chloride with hexamethyldisilane. This is an adaptation of the procedure for tetrachlorodimethyldisilane.[9]

In the course of our work, we also desired a silylating agent that would produce less swelling than DMAPMDS. We decided to synthesize the "smaller" N,N-dimethylamino-1,2-dimethyldisilane (DMADMDS). This material is moisture-sensitive but not pyrophoric. While many of the synthetic routes examined did provide the product, they often were not amenable to scale up or provide for adequate purification. Equation 2 shows a synthesis of DMADMDS. An aromatic ring is used to protect one of the halogens of 1,2-dimethyltetrachlorodisilane[10] during reduction by lithium aluminum hydride. Addition of phenyl magnesium bromide to 1,2-dimethyltetrachlorodisilane provides phenyl-1,2-dimethyltrichlorodisilane which is reduced without isolation which provides phenyldimethyldisilane in almost 85% isolated yield. The phenyl group of phenyldimethyldisilane can be removed by many routes including anhydrous HBr at -78 °C.[11] However, careful Schlenk or high vacuum techniques must be employed. Additionally, rigorous control of the reaction time, starting material purity, and other reaction conditions is needed in order to avoid pyrophoric by-products. Aminolysis provided DMADMDS in 54% overall yield from phenyldimethyldisilane.

Results:

The low boiling point of DMADMDS (110 °C) allows use of lower temperatures during silylation. DMADMDS also causes less swelling of the polymer network (65% theoretical volume increase for a pure cresol novolac) upon silylation than does DMAPMDS (100%). The calculated swelling associated with DMADMDS is identical to that of a trimethysilyl group. DMADMDS yields a silylated polymer with a higher weight percent of silicon (26.8%, calculated for complete silylation of a pure cresol novolac) as compared to DMAPMDS, (22.3%). The increased weight percent silicon provides greater etch selectivity and increased processing latitudes during reactive ion etching, RIE. However, imaging results with this material have not been as good as expected. DMADMDS diffuses into the crosslinked areas of the photoresist during silylation. This lowers the silicon contrast and consequently the imaging quality.

DMAPMDS diffuses through a layer of photoresist XP-8844 in much the same manner as do other silylated agents.[12] Rutherford backscattering (RBS) data (Figure 3) indicate that the diffusion of DMAPMDS is non-Fickian. Sharp delineation between the unsilylated and silylated regions is always observed. This indicates that under the conditions employed for the silylation step, DMAPMDS

reacts very rapidly with the resin relative to its diffusion rate. RBS data indicate that the planarizing layer used is not silylated. This prevents silicon from diffusing under exposed regions. Diffusion of silicon under the crosslinked areas can cause loss of line width control.[13] Figure 2 is a standard contrast curve from early studies in our process development. It indicates that the contrast is very high and, as expected, is related to the degree of overetch. More silicon incorporation increases overetch latitude and the contrast as well.

An important observation was that the DMAPMDS produced via the two different routes (SA and TA) gave very different results. Silylations using material prepared via triflic acid were more rapid than silylations using material produced via the sulfuric acid method. Additionally, the lithographic patterns achieved with the triflic acid material were much poorer than those produced with the sulfuric acid material. We suspected that the reason for the differences might be due to an impurity in the SA produced material.

Synthesis of chloropentamethyldisilane (b.p. 134 °C) from sulfuric acid and ammonium chloride as described in the literature required two distillations in order to separate the product, chloropentamethyldisilane, from the unreacted hexamethyldisilane and 1,2-dichlorotetramethyldisilane (b.p. 148 °C) which forms during a competing, second protonolysis as shown in Equation 3. The protonolysis of the first methyl group is claimed to be 10 times faster than the protonolysis of the second methyl group. We found the rates differed by a factor of 5. The similarity of the boiling points of chloropentamethyldisilane and 1,2-dichlorotetramethyldisilane complicates the separation and suggested that SA produced DMAPMDS might be contaminated with a small amounts ~1% of 1,2-bis(N,N-dimethylamino)tetramethyldisilane. We verified its presence and quantified the amount of 1,2-bis(N,N-dimethylamino)tetramethyldisilane by GC and NMR. In order to unambiguously determine that small amounts of difunctional disilane and crosslinking were the source of the differences, we added 1-2 percent of bis(dimethylamino)dimethylsilane, another bifunctional crosslinking silane, to pure TA produced DMAPMDS. This addition restored resolution similar to that of the SA produced DMAPMDS. Finally, we synthesized 1,2-bis(N,N-dimethylamino)tetramethyldisilane and added it to the TA prepared DMAPMDS, again restoring resolution. We believe that small percentages of crosslinker in the DMAPMDS decrease flow of the silylated regions by lightly crosslinking the silylated regions and raising the T_g of the silylated resist. This increase in T_g, modulus, and viscosity due to crosslinking helps ensure that the volume increase is

anisotropic. This is shown clearly in the SEM's of cross-sectioned wafers that were silylated with different batches of DMAPMDS, Figure 4.

Discussion:

Flow in silylated resists was identified as a problem very early in the development of silylation imaging schemes. The reduction of T_g upon silylation and the associated volume increase make flow very likely. A number of different techniques to deal with this flow problem have been developed. They range from techniques to prevent flow during silylation to techniques to remove the effects of flowed resist afterwards. These techniques include plasma descuming[14] and partial solution development of the wafer prior to silylation.[15] Presilylation aqueous development can be used to create a channel in which the silylated resist expands.[16] While all of these schemes contribute to alleviating the effects of silylated resist flow, we feel that the presence of the crosslinker in the disilane silylating agent during silylation achieves the same results, but with a simplicity that the multistep methods can not match.

The significance of the crosslinker is that it dramatically modifies the lithographic behavior even in low concentrations. We believe that this is the first example of using small amounts of vapor phase crosslinking agents to control flow during silylation, but this is certainly not the first example of the use of bifunctional reagents. The use of bifunctional silylation reagents such as hexamethylcyclotrisilazane has been reported previously.[17] Typically, these materials are used in solution silylation schemes as they are not very volatile.[18] A comparison of solution and vapor phase silylation has been made.[19] Bifunctional reagents consume up to two phenolic OH's for every reagent molecule, resulting in less silicon incorporation, lower etching selectivity, lower silicon contrast and narrower processing windows. Previous use of crosslinking silylating agents has employed them either as the sole component in silylation or in a single step of a two step silylation prior to silylation with monofunctional silylation reagents. By employing only a small amount of crosslinker, fewer phenolic sites bind to the same silylating agent. This results in more silicon in the photoresist and increased etching selectivity and silicon contrast. Use of pure monosilicon difunctional crosslinker would result in decreased silicon in the silylated polymer since two phenolic sites are used per each silicon agent.

The CARL process addresses this problem by using bifunctional oligomers containing multiple silicon atoms.[20] The oligomers are bifunctional, having a reactive amine group at each end of the chain, and deliver multiple silicon atoms to

each binding site in the polymer. However, the oligomers are so large that a great deal of additional organic material is delivered and much greater swelling occurs. This results in the swelling and line feature expansion that is the distinctive feature of the CARL process.

A two step silylation process to control flow that also employs crosslinking has been discussed.[21] In this process, the imaging layer is first presilylated by bis(dimethylamino)dimethylsilane in the gas phase to form a crosslinked "skin" on the surface of the resist that inhibits flow during the second silylation step which employs a monofunctional reagent. Our single step crosslinking silylation process is similar, but offers the advantages of simplicity (1 step) and increased silicon content due to the significantly lower level of crosslinker and use of disilane silylation reagents.

In order to test the utility of the silylation techniques that we have developed, we have extensively examined cross-sectioned and plasma-stained samples of wafers in order to learn more about the effect of the crosslinker concentrations on imaging results. Figure 4 shows the effect of the crosslinker in DMAPMDS on 0.30 μm equal lines and spaces after silylation and oxygen plasma development in a helicon etcher. With pure DMAPMDS made by the TA method, the surface of the silylated top layer was planarized by flow, Figure 4B. With SA prepared DMAPMDS the swelling was still evident but was much more anisotropic, Figure 4A. The effect of this difference in silicon contrast on the patterns developed after descum and oxygen plasma etching is dramatic. The sidewalls have less undercut for material silylated with the TA produced DMAPMDS, Figure 4D. This anisotropy results from erosion of the thin silylated masking layer during etching. It occurs because there is less silicon present at the edges of features. As the edges of the masking layer are slowly etched away, any undercut is rendered invisible because the silicon mask lateral erosion rate is comparable to the undercut rate. Although this affords attractive micrographs, it causes poor CD control during overetch. Additionally, erosion of the masking layer will cause feature size and feature geometry nonlinearities. The micrographs in Figure 4C clearly show undercut due to etching by neutrals which are responsible for isotropic etching. Features such as these, Figure 4C, would be unacceptable for device manufacture.

In order to improve the imaging and decrease undercut, which is clearly present in Figure 4C, we examined etching conditions that afforded sidewall deposition during etching. Again the effect of the crosslinker is dramatic. In Figure 5, 0.25 μm line and space patterns silylated with and without crosslinker were etched

with SO_2 and O_2 under our improved etching conditions. Under these new conditions with a 50% overetch, the patterns silylated with TA produced DMAPMDS do not develop at all, while those silylated with DMAPMDS containing crosslinker develop and have straight sidewalls. Integration of all of these advance (disilane silylation agents containing a few percent of crosslinking disilane, and etching conditions that afford sidewall deposition) provides a surface imaging scheme that is very reproducible and capable of very high quality features. Figure 7 shows three micrographs of line and space patterns developed using this integrated process. The three micrographs in Figure 7 (0.30, 0.25 and 0.20 μm line and space patterns) were all achieved with identical doses, 38 mJ/cm^2.

To address the resolution limits of this dry-developed imaging system, we examined wafers exposed at 13.5 nm (EUV). Figure 6 shows 0.20 μm and 0.15 μm lines and spaces obtained by EUV exposures. The EUV images are inferior to the DUV 248 nm images (Figure 7 contains 0.20 μm line and space patterns) even though the EUV images should have resolved features as small as 80 nm. Experiments with 60 nm thickness films of ZEP-320 have given even poorer results than those obtained with our dry developed scheme.[22] This suggests that the resolution is not resist limited, but rather is aerial image limited. At this point we can only say that our silylated resist is capable of a least 150 nm resolution.

Silylating Agent	Binding Group	b.p. (°C)	Weight % Silicon	Volume Increase (%)	Etching Selectivity
Me_3SiNMe_2	$-SiMe_3$	86	14.6	71	18
$Me_2HSiNMe_2$	$-SiHMe_2$	67	15.7	47	27
$Me_5Si_2NMe_2$	$-Si_2Me_5$	155	22.4	124	45
$Me_2Si_2H_3NMe_2$	$-Si_2Me_2H_3$	125	26.9	71	~60
$Me_2Si_2H_3NEt_2$	$-Si_2Me_2H_3$	147	26.9	71	~60
Difunctional Silylating Agents:					
$*(Me_2N)_2SiMe_2$	$-SiMe_2-$	128	9.5	21	~10
$*(Me_2N)_2SiMeH$	-SiMeH-	112	9.9	12	~10
$*Me_4Si_2(NMe_2)_2$	$-Me_4Si_2-$	192	15.8	47	~15

Table 1: Commonly used silylation agents and properties. Weight percent silicon was calculated by assuming complete silylation of a cresol novolac. Volume Increase was calculated as atom percent increase in a cresol novolac. Reagents marked with an * are difunctional. Etching selectivity is silylated resist vs. hard baked photoresist etched under the following conditions: source power, 2500 W; chuck power, 75 W; pressure, 2.5 mTorr; flow, 100 sccm O_2; temperature, 25 °C.

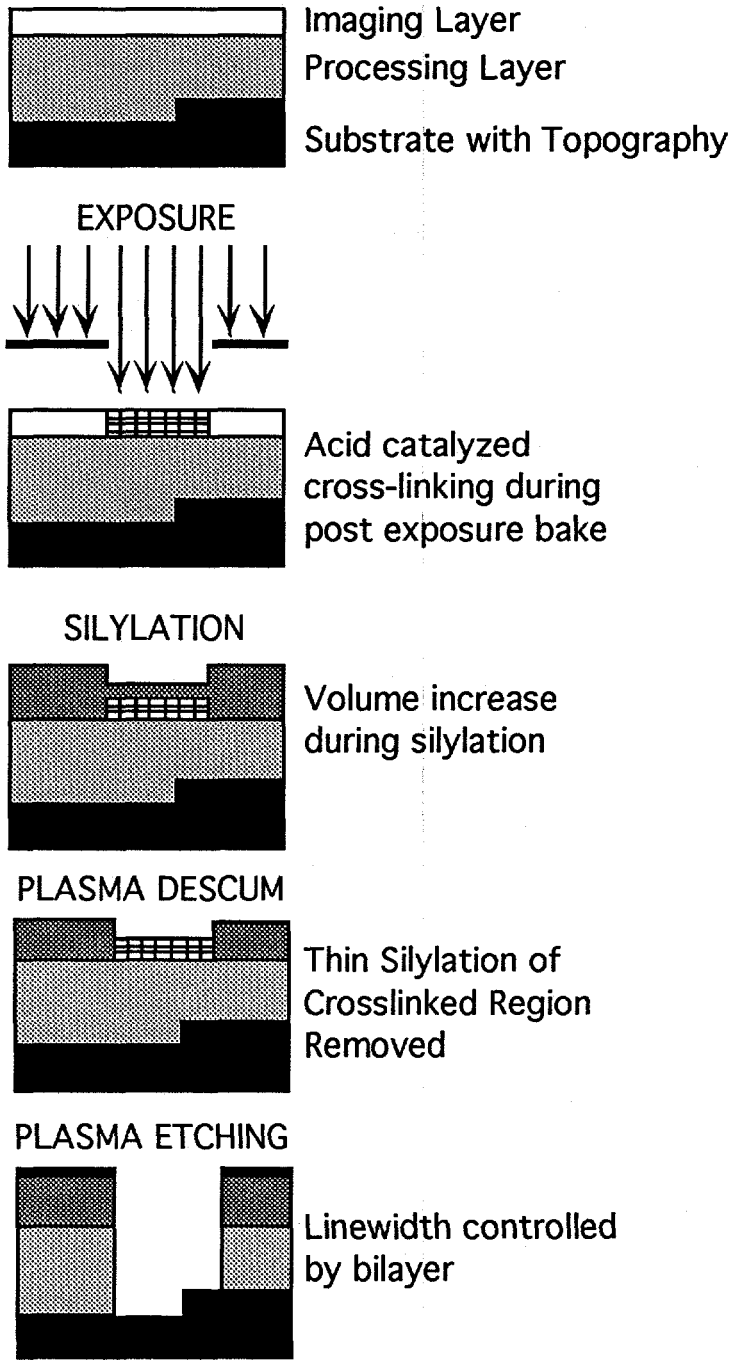

Figure 1: Schematic of bilayer silylation process using disilanes.

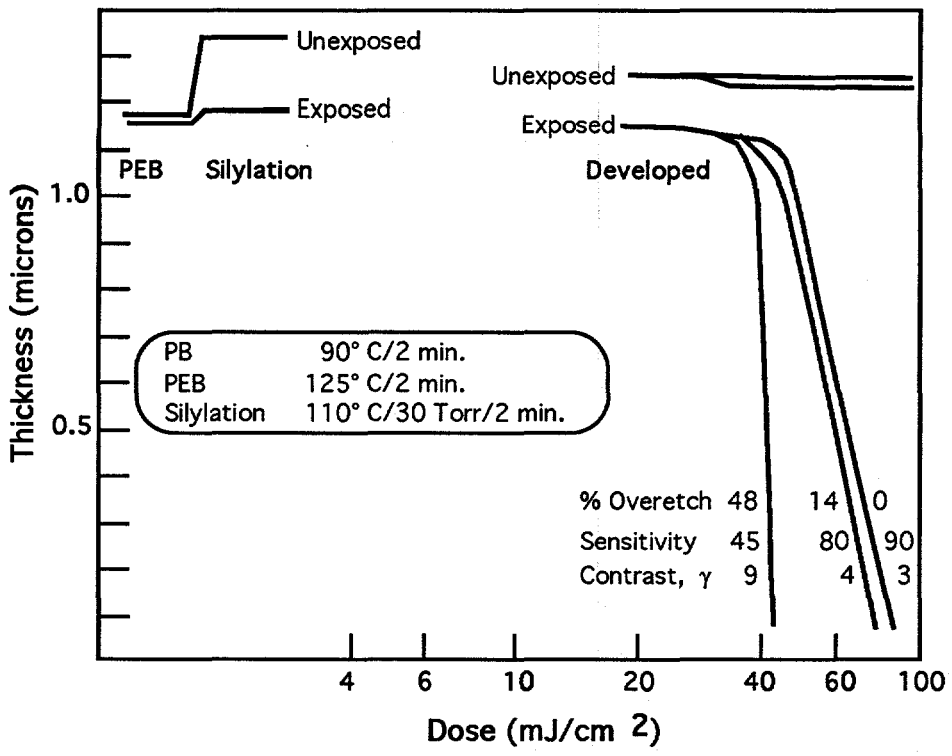

Figure 2: Effect of overetch on the sensitivity and contrast of the XP-8844/SPR 1811 bilayer resist system. Silylation conditions were 110 °C for 2 min. at 30 Torr DMAPMDS. Development used Helicon etching with a source power of 2500 Watts, chuck power of 75W, 25 °C, 2.5 mTorr, 100 sccm oxygen. The initial film thickness was 1.1 μm. Post exposure bake (PEB) was 125 °C for 2 minutes. Prebake (PB) was 2 minutes at 90 °C. The percentage of overetch is indicated along with the sensitivity (mJ/cm^2) and contrast (γ).

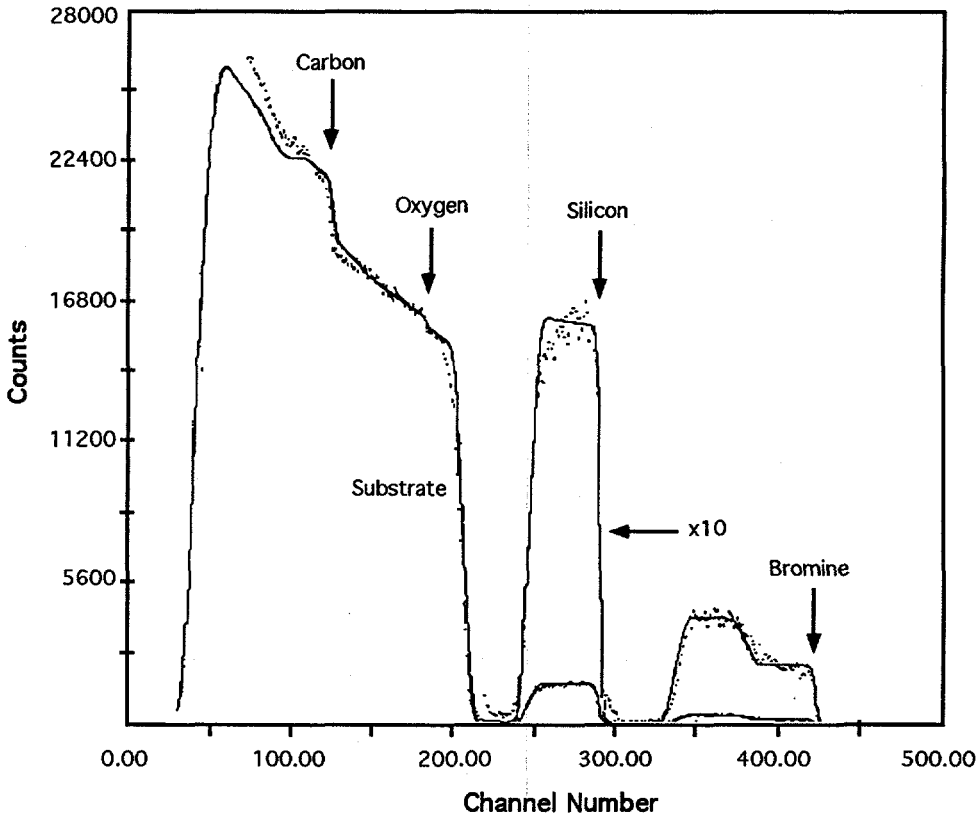

Figure 3: RBS data from a partially silylated (DMAPMDS) thick film of Shipley XP-8844, (XP-8844 is the imaging layer shown in Figure 1).

Figure 4: The effect of crosslinker on silylation with DMAPMDS on 0.30 μm lines and spaces, cleaved and stained. A) Top left: silylation with crosslinker present. B) Top right: silylated without crosslinker present, flow evident. C) Lower left, patterns resolved after descuming and oxygen plasma etching of silylated patterns containing crosslinker. The undercut results since there is less erosion of the silicon masking layer and the effect of neutrals is observed. D) Lower right, patterns resolved after descuming and oxygen plasma etching of patterns silylated without crosslinker. The masking layer erodes at rate comparable to the undercut rate giving straight sidewalls but CD control is harder.

Figure 5: The effect of the crosslinker on 0.25 μm lines and spaces images silylated with DMAPMDS using SO_2/O_2 etching conditions that afford sidewall deposition during etching. The patterns at right were silylated without crosslinker and did not develop. The images at left were achieved with the crosslinker present and have straight sidewalls. A 50% overetch was used.

Figure 6: EUVL (13.5 nm) exposures of 0.20 μm and 0.15 μm line and space patterns developed using DMAPMDS containing a crosslinker and using the improved etching conditions with a dose of 24 mJ/cm^2.

Figure 7: DUV exposures of 0.30 μm, 0.25 μm, and 0.20 μm line and space patterns developed using DMAPMDS with 5% weight percent of 1,2-bis(N,N-dimethylamino)tetramethyldisilane present and developed with SO_2/O_2 etching conditions that afford sidewall deposition during etching. A 50% overetch was employed. All features were printed with the same dose, 38 mJ/cm^2.

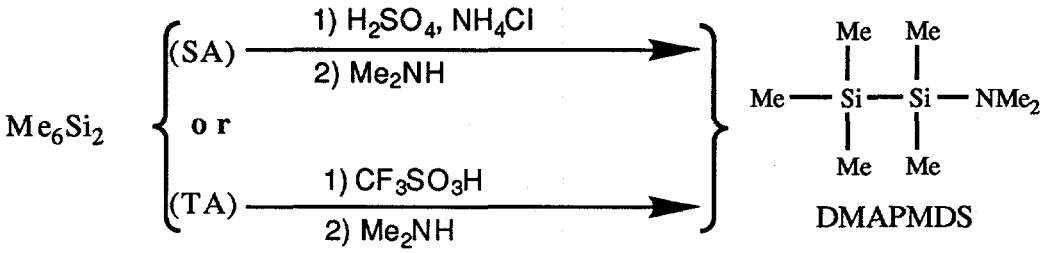

Equation 1: Two routes to DMAPMDS, SA and TA.

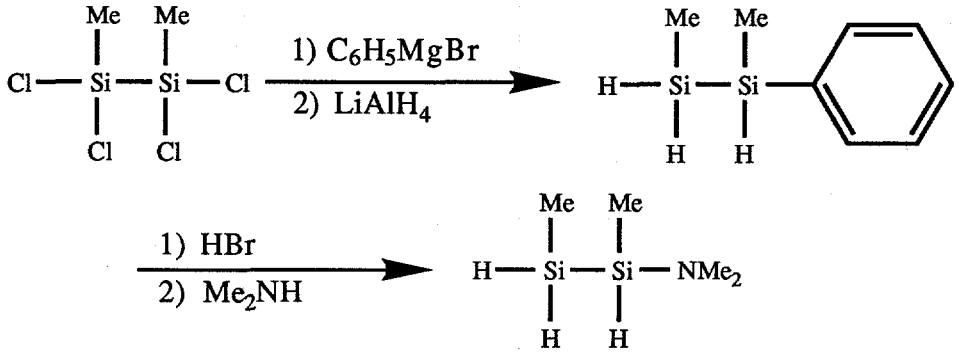

Equation 2: Synthesis of DMADMDS.

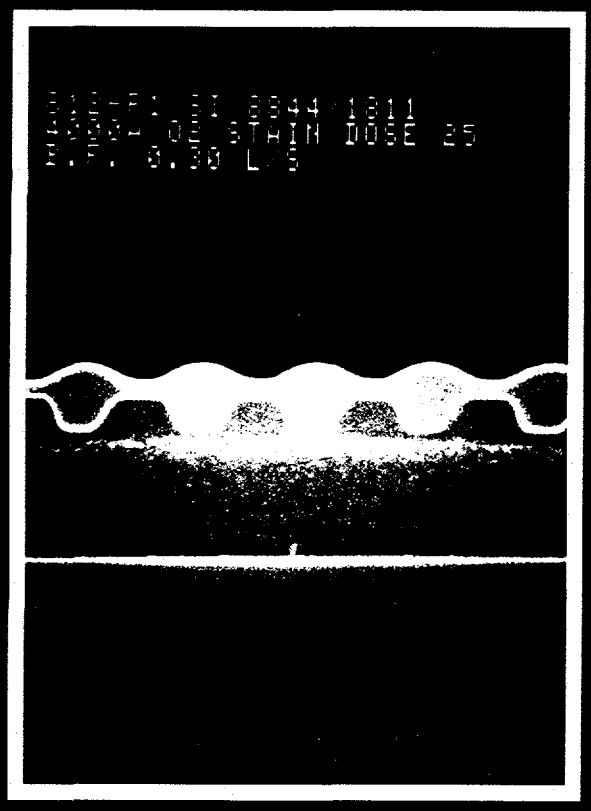

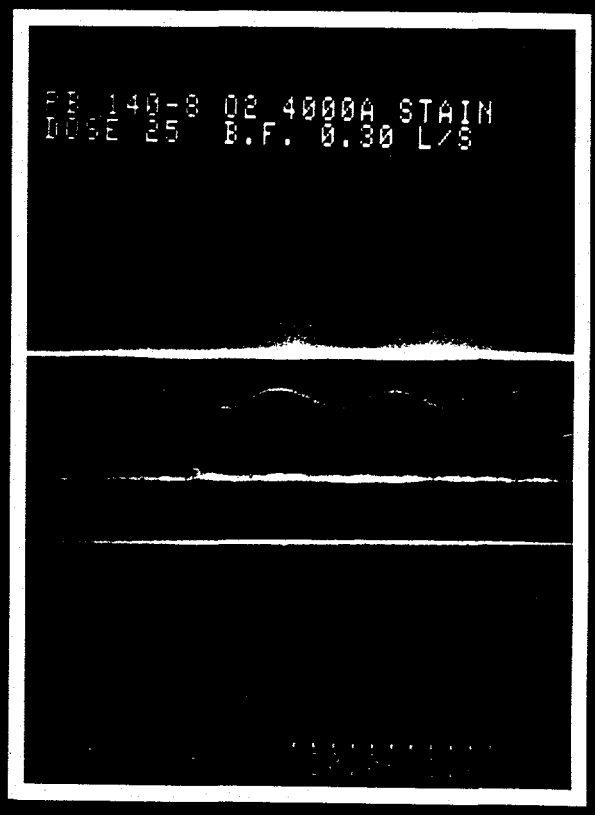

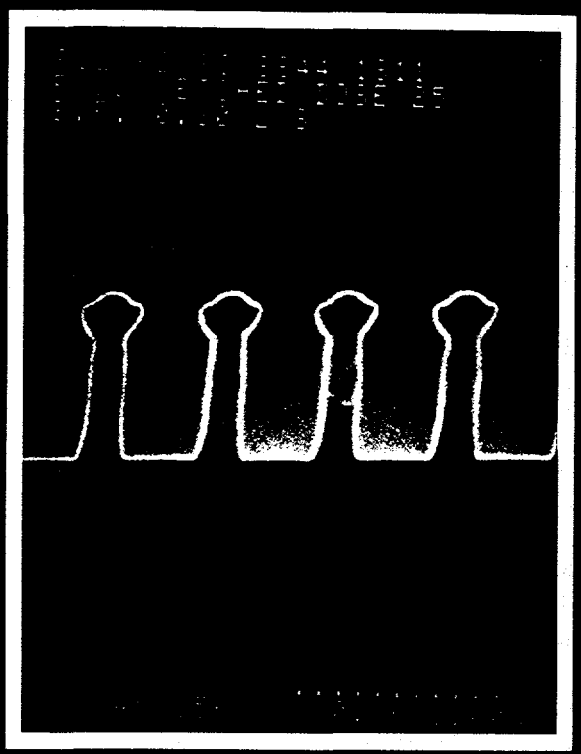

E95-0058 depARTment 12616

Fig #4

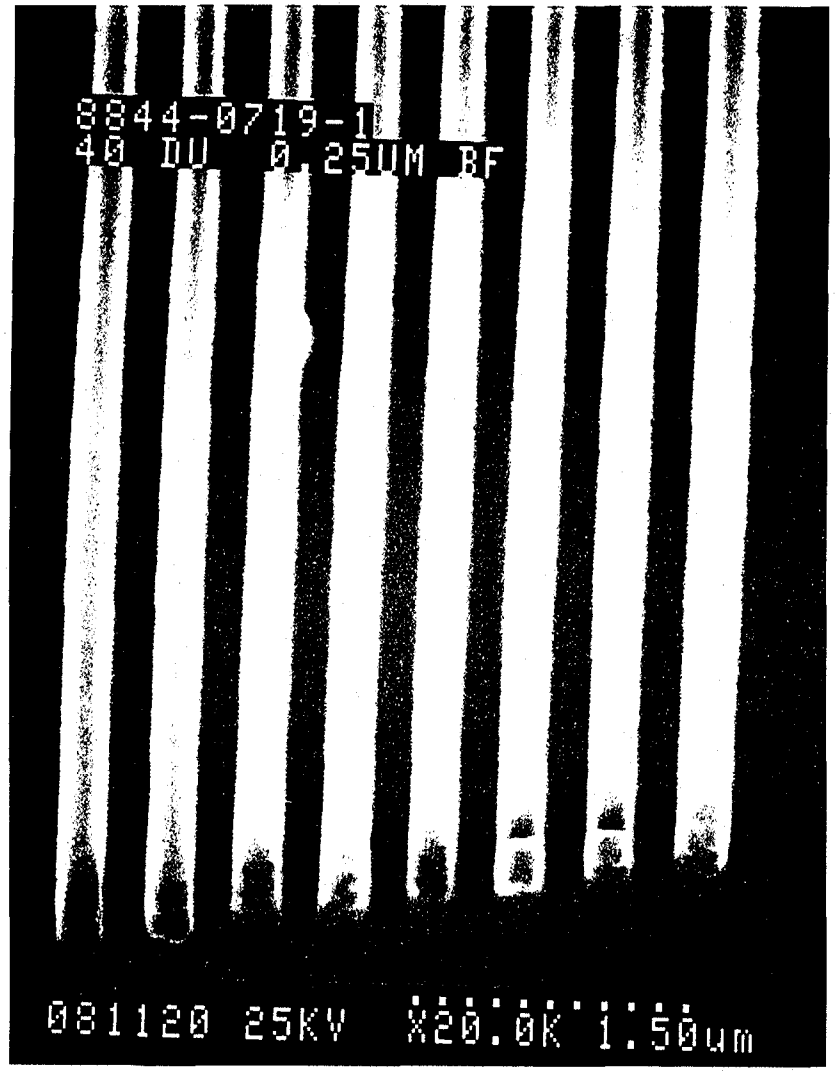

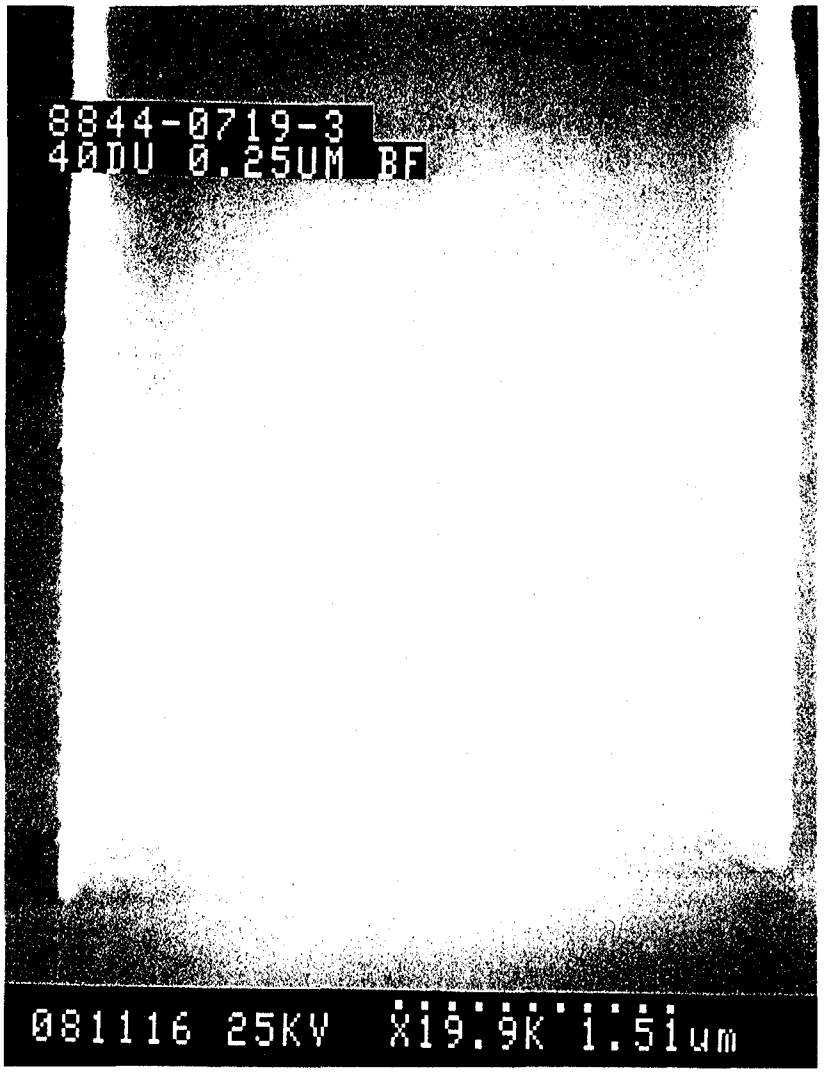

Fig 5

Sandia National Laboratories

E94-0728

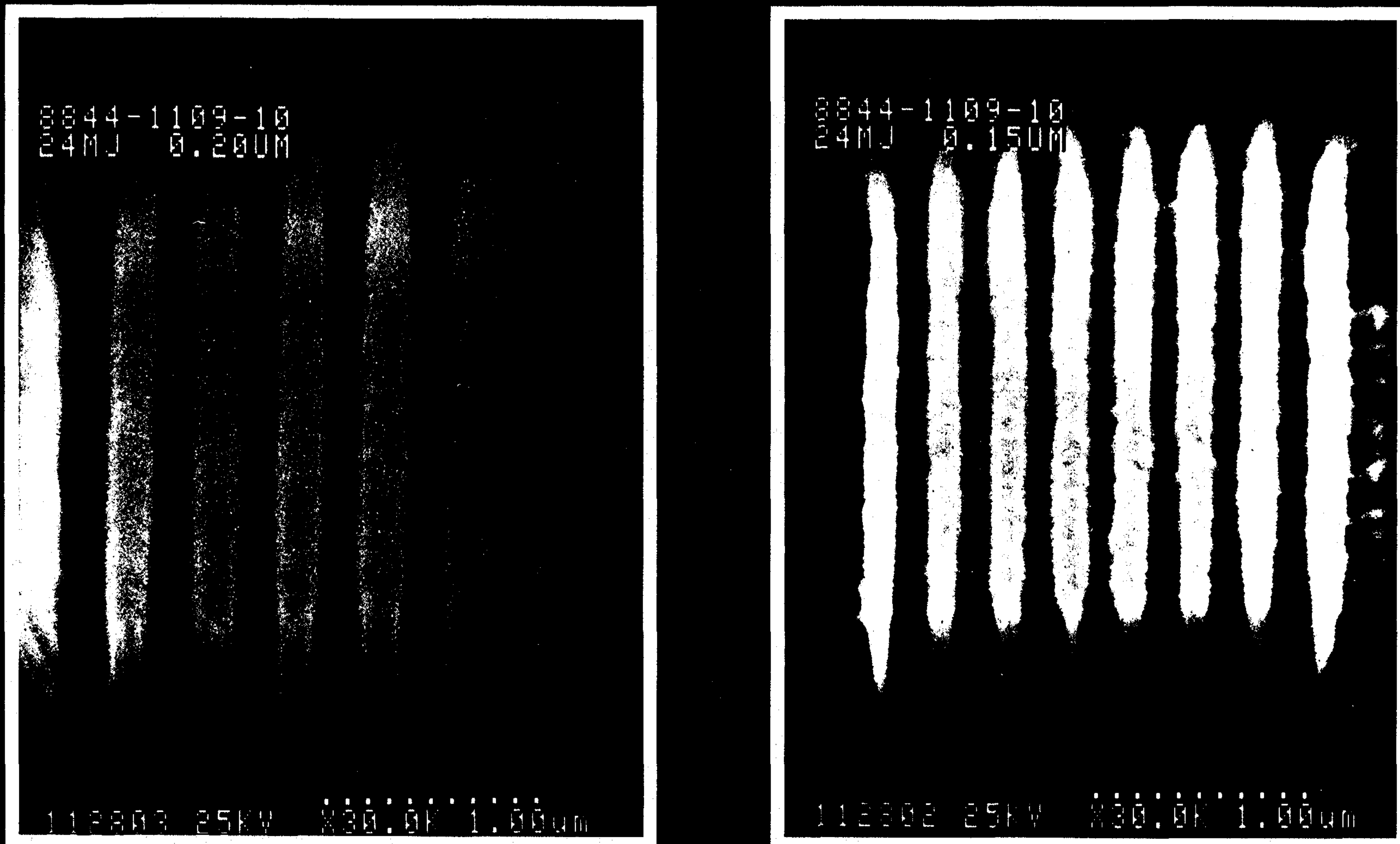

E95-0057 depARTment 12616

Fig 6

E95-0055

depARTment 12616

Fig 7

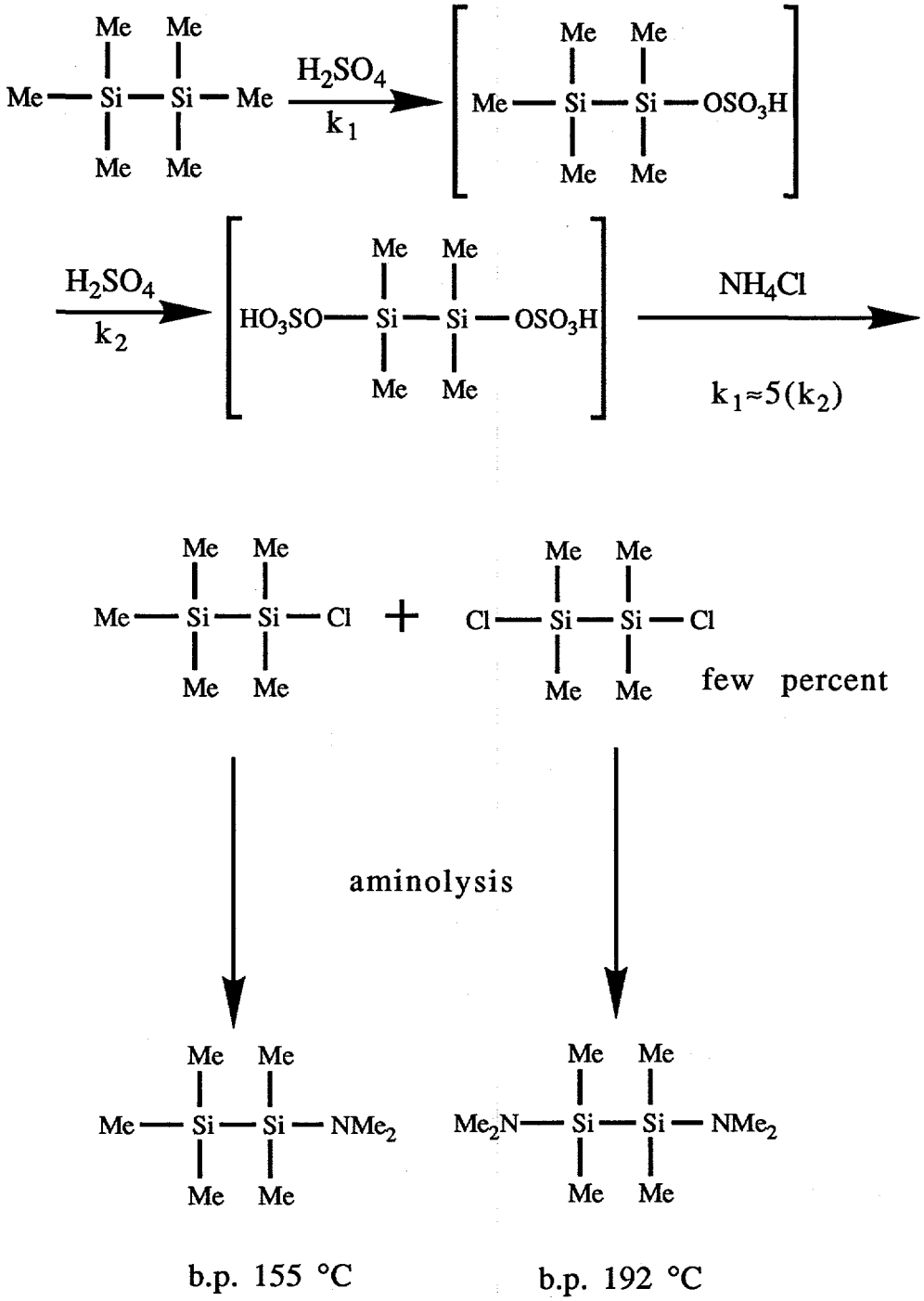

Equation 3: Synthesis of DMAPMDS and origin of the crosslinker 1,2-bis(dimethylamino)tetramethyldisilane.

[1]This work was performed at Sandia National Labs supported by the U.S. Department of Energy under contract DE-AC04-94AL85000.

[2](a) Coopmans, F.; Roland, B. *Proc. SPIE*, **1986**, *631*, 34. (b) Garza, C. M.; Misium, G. R.; Doering, R. R.; Roland, B.; Lombaerts, R. *Proc. SPIE*, **1989**, *1086*, 229.

[3](a) Thackery, J. W.; Bohland, J. F.; Pavelchek, E. K.; Orsula, G. W.; McCullough, A. W.; Jones, S. K.; Bobbio, S. M. *Proc. SPIE*, **1989**, *1185*, 2-11. (b) Pavelchek, E. K.; Bohland, J. F.; Thackery, J. W.; Orsula, G. W.; Jones, S. K.; Dudley, B. W.; Bobbio, S. M.; Freeman, P. W. *J. Vac .Sci. Technol.* **1990**, *B8*, 1497-1501.

[4]Calvert, J. M.; Koloski, T. S.; Dressick, W. J.; Dulcey, C. S.; Peckerar, M. C.; Cerrina, F.; Taylor, J. W.; Suh, D.; Wood II, O.R.; MacDowell, A. A.; D'Souza, R; *Optical Engineering*, **1993**, *32(10)*, 2437-2445.

[5]Wheeler, D. R.; Hutton, R.; Boyce, C.; Stein, S.; Cirelli, R.; Taylor, G. *Proc. SPIE* , **1995**, *2438*, 762.

[6]Taylor, G. N.; Hutton, R. S.; Stein, S. M.; Boyce, C. H.; Wood, O. R.; LaFontaine, B.; MacDowell, A. A.; Wheeler, D. R.; Kubiak, G. D.; Ray-Chaudhuri, A. K.; Berger, K.; Tichenor, D. *Proc. SPIE*, **1995**, *2437*, 308.

[7](a) Dubowchik, G. M.; Gottschall, D. W.; Grossman, M. J.; Norton, R. L.; Yoder, C. H. *J. Am. Chem. Soc.*, **1982**, *104*, 4211-14. (b) Engelhardt, G.; Radeglia, R.; Kelling, H.; Stendel, R. *J. Organomet. Chem.* **1981**, *212(1)*, 51-8. (c) Hengge, E.; Pletka, H. D.; Hoefler, F. *Monatsh. Chem.*, **1970**, *101(2)*, 325-36. (d)Kumada, M.; Yamaguchi, M.; Yamamoto, Y.; Nakajima, J.; Shhna, K. *J. Org. Chem.* **1956**, *24*, 1264-1268.

[8](a) Matjaszewski, K.; Chen, Y. L. *J. Organometallic Chem.* **1988**, *340*, 7-12. (b) Bassindale, A. R.; Stout, T. *J. Organometallic Chem.* **1984**, *271*, C1-C3.

[9]Sakurai, H.; Watanabe, T.; Kumada, M. *J. Organometallic Chem.*. **1967**, *7*, P15-P16.

[10](a) Watanabe, H.; Kobayashi, M. Koike, Y.; Nagashima, S.; Matsumoto, H.; Nagai, Y. *J. Organometallic Chem.* **1977**, *128*, 173-175. (b) Sakurai, H.; Watanabe, T.; Kumada, M. *J . Organometallic Chem.* **1967**, *7*, P15-P16.

[11](a) Schmidbauer, H.; Zech, J.; Rankin, D. W. H.; Robertson, H. E.; *Chem. Ber.* **1991**, *124*, 1953-1956. (b) Hager, R. Steigelmann, O.; Müller, G. Schmidbauer, H. *Chem. Ber.* **1989**, *122*, 2115-2119.

[12](a) Hartney, M. A.; Rothschild, M.; Kunz, R. R.; Ehrlich, D. J.; Shaver, D. C. *J. Vac. Sci. Technol.* **1990**, *B 8(6)*, 1476-1480. (b) Baik, K.; Van den hove, L.; Goethals, A. M.; Op de Beeck, M; Roland, B. *J. Vac. Sci. Technol.* **1990**, *B 8(6)*, 1481-1487.

[13]Baik, K-H.; Ronse, K.; Van den Hove, L.; Roland, B. *Proc. SPIE*, **1993**, *1925*, 302.

[14]Goethals, A. M.;Baik, K.H.; Van den hove, L.; Tedesco, S. *Proceedings SPIE*, **1991**, *1466*, 604.

[15]Pavelchek, E. K.; Calabrese, G. S.; Bohland, J. ; Dudley, B. W. ; Jones, S. K. ; Freeman, P. W. *Optical Eng.* **1993**, *32(10)*, 2376.

[16]W. Han, W.; Lee, J.; Park, J. ; Park, C.; Kang, H.; Koh, Y.; Lee, M. *Proceedings SPIE* , **1993**,*1925*, 291.

[17]Shaw, J. M.; Hatzakis, M.; Babich, E. D.; Paraszczak, J. R.; Witman, D. F.; Stewart, K. J. *J. Vac. Sci. & Technol. B* , **1989**, *7*, 1709.

[18]Baik, K-H.; Ronse, K.; Van den Hove, L.; Roland, B. *Proc. SPIE*, **1993**, *1925*, 302.

[19]Hartney, M. A.; Kunz, R. R.; Eriksen, L. M.; LaTulipe, D. C. *Optical Eng.* **1993**, *32(10)*, 2382.

[20]Sebald, M.; Bertold, J.; Beyer, M.; Leuschner, R.; Nölscher, Ch.; Scheler, U.; Sezi, R.; Ahne, H.; Birkle, S. *Proceedings SPIE*, **1991**, *1466*, 227.

[21]Pavelchek, E. K.; Calabrese, G. S.; Bohland, J. ; Dudley, B. W. ; Jones, S. K. ; Freeman, P. W. *Optical Eng.* **1993**, *32(10)*, 2376.
[22]Taylor, G.N.; Hutton, R. S.; Stein, S. M.; Boyce, C. H.; LaFontaine, B.; MacDowell, A. A.; Wheeler, D. R. *Proceedings SPIE*, **1995**, *2437*, 308.